catalysts

MDPI

Article

Improved Light Hydrocarbon, Furans, and BTEX Production from the Catalytic Assisted Pyrolysis of *Agave salmiana* Bagasse over Silica Mesoporous Catalysts

Leoncio Santiago-Martínez [1], César Irán González-Falcón [1], Jaime Reyes-Hernández [2], Brent E. Handy [1] and María-Guadalupe Cárdenas-Galindo [1,*]

[1] Facultad de Ciencias Químicas, Universidad Autónoma de San Luis Potosí, Av. Dr. Manuel Nava No. 6, Zona Universitaria, San Luis Potosí 78210, S.L.P., Mexico
[2] Facultad de Enfermería, Universidad Autónoma de San Luis Potosí, Av. Niño Artillero No. 130, Zona Universitaria, San Luis Potosí 78210, S.L.P., Mexico
* Correspondence: cardenas@uaslp.mx; Tel.: +52-444-826-2440 (ext. 6468)

Abstract: The pyrolysis of the biomass *Agave salmiana* bagasse (10 K/min, ambient to 700 °C) was investigated in the absence and presence of Aerosil and MCM-41 catalysts. MCM-41 was synthetized using a typical hydrothermal method and characterized with XRD, SAXS, SEM, TEM, and nitrogen physisorption to confirm the presence of unidimensional 3.4 nm diameter pores. Pyrolysis products were monitored online with mass spectrometry (MS), analyzing the production of 29 different compounds, clustered in several groups, namely, olefins (ethene, 2-butene, 1,3-butadiene), oxygenated compounds (methanol, 2-methylbutanol, acetic acid), furan derivatives (furan, furfural, 2-methylfurane), and aromatic compounds (BTEX). Complete decomposition of the cellulose and hemicellulose content of the biomass was observed at temperatures below 400 °C. Lignin decomposition was completed by 550 °C. Catalyst-assisted pyrolysis showed reduced acetic acid and methanol formation with Aerosil and MCM-41. The use of Aerosil does not affect the overall production of olefins, yet increases benzene yield, while reducing the production of phenol, furan, and furan derivatives. With MCM-41, there is increased production of olefins, furan, furan derivatives, cyclohexanone and BTEX, yet phenol production is decreased. At temperatures below 400 °C, the product formation pattern is comparable to non-catalytic pyrolysis.

Keywords: catalytic pyrolysis; MCM-41; *Agave salmiana* bagasse; furan; Aerosil 380

check for updates

Citation: Santiago-Martínez, L.; González-Falcón, C.I.; Reyes-Hernández, J.; Handy, B.E.; Cárdenas-Galindo, M.-G. Improved Light Hydrocarbon, Furans, and BTEX Production from the Catalytic Assisted Pyrolysis of *Agave salmiana* Bagasse over Silica Mesoporous Catalysts. *Catalysts* **2023**, *13*, 548. https://doi.org/10.3390/catal13030548

Academic Editors: Karine De Oliveira Vigier and Mickael Capron

Received: 31 January 2023
Revised: 1 March 2023
Accepted: 3 March 2023
Published: 9 March 2023

Copyright: © 2023 by the authors. Licensee MDPI, Basel, Switzerland. This article is an open access article distributed under the terms and conditions of the Creative Commons Attribution (CC BY) license (https://creativecommons.org/licenses/by/4.0/).

1. Introduction

Lignocellulosic biomasses have received considerable attention as promising feedstocks to obtain fuels and chemicals. Furthermore, their use could contribute to mitigate greenhouse gas emissions [1–3]. Particularly, residual lignocellulosic biomasses are attractive for these applications since they do not compete directly with food production. This is the case with Agave bagasse, a lignocellulosic agro-industrial residue of the production of tequila and mezcal, alcoholic beverages produced from *Agave tequilana Weber* and *Agave salmiana*, respectively [4,5].

Agave spp. are native of the Americas but have been introduced around the world (Australia, Brazil, Tanzania, Kenya, Madagascar, China) for commercial use, especially for fiber and beverage production [4–6]. Mexico presents the highest diversity of Agave species, with higher productivity levels in semiarid regions, and a large area cultivated with *Agave tequilana Weber*, and *Agave salmiana* [6]. It has been reported that *Agave tequilana Weber* generates approximately 20 kg of bagasse (wet basis) for each liter of tequila, while *Agave salmiana* produces 15–20 kg of bagasse (wet basis) for each liter of mezcal [7,8]. This represents 10 million tons of *Agave tequilana* bagasse (wet basis), and 125,000 tons of *Agave salmiana bagasse* (ASB) (wet basis) every year, estimation based on the total volume

of tequila produced during 2021 [9] and mezcal produced in México during 2019 [9,10]. Mezcal production has dramatically increased (800%) from 2012 to 2022 due to increases in both domestic and foreign mezcal consumption. Consequently, the concomitant increase in solid residue (bagasse) generation must be dealt with, since its disposal has a negative environmental impact on both soil and water [11,12]. Until now, the most common use of agave bagasse is as forage for animals [13], in the compost mixture formulation to increase soil acidity, and in combustion to produce heat and power [6]. Therefore, alternative applications of agave bagasse should be explored to produce high added value products, such as energy, fuels, and chemicals.

Pyrolysis is a thermochemical pathway that can be used for agave bagasse decomposition, in addition to combustion and gasification [8–14]. During pyrolysis, the thermal decomposition of lignocellulosic biomass occurs in absence of air, to obtain gas, bio-oil, and char products. A biomass with highly volatile matter and low ash content is desirable for this process to yield an elevated conversion to high-value chemical products, and to reduce char formation [14]. *Agave bagasse* is composed of approximately 40–73% of cellulose, 4–20% of hemicellulose, and 7–20% of lignin [4–6,12,15–17], depending strongly on environmental conditions, as well as the region where it is produced [6]. ASB has a low content of lignin and a high content of amorphous cellulose compared to woody biomasses [4]. These characteristics may be beneficial to obtain high bio-oil yields in ASB pyrolysis.

The bio-oil is the main product of pyrolysis, and a potential substitute of gasolines, diesel, or jet fuel. Nevertheless, bio-oil is a corrosive mixture of up to 350 different compounds with low energy density properties, due to the high content of oxygenated compounds and elevated acidity, that limits its direct utilization in internal combustion engines [1]. The yield to char, bio-oil, and gas during pyrolysis is highly dependent on pyrolysis conditions, especially temperature and heating rate, with the liquid fraction favored at temperatures between 500 °C and 550 °C, slow heating rate, and short residence time (few seconds to few minutes) of vapor products in the reactor [18]. However, a high yield to the liquid fraction does not result in a higher quality bio-oil since it may have a high content of oxygenated compounds and tar. Tar is composed of biomass fragments of high molecular weight, mainly aromatics, and includes complex aromatic polycyclic hydrocarbons, phenolic ethers, alkylphenols, and heterocyclic ethers [19]. Tar can cause operational problems in pyrolysis and gasification processes, due to condensation in the downstream units [19]. Thus, bio-oil upgrading is necessary to produce a bio-oil with a low oxygen content and rich in light hydrocarbons.

The bio-oil quality can be improved using acid catalysts to increase the selectivity to desired products and favor deoxygenation processes. HZSM-5 zeolites, and their modifications with Fe, reduce the formation of oxygenated compounds, such as acids, alcohols, esters, furans, and ketones; improve the selectivity to BTEX, aliphatic hydrocarbons, and some light olefins; additionally, they promote the formation of naphthalene derivatives [20,21]. A disadvantage of these materials is their microporosity, since the large biomass fragments produced by thermal decomposition are diffusion-limited in these pores. Excessive cracking of these fragments within the micropores leads to high coke formation.

Diffusion limitations can be eliminated with mesoporous materials such as MCMs and SBA-15. Kelkar et al. studied upgrading of poplar pyrolysis products with sulfated zirconia supported on MCM-41 and found improvement of deoxygenation activity when compared with the non-catalytic pyrolysis, but with the production of significantly less BTEX than HJZSM-5 [21]. Physical mixtures MCM-41/ZSM-5 [22], and Al-MCM-41/H-ZSM-5 [23] have been proposed as alternatives to mitigate the coke formation and to promote the cracking of large molecules into small molecules, due to the large pore size, and mild acidity present in MCM-41 type materials. Consequently, desired characteristics of pyrolysis catalysts in addition to thermal and hydrothermal stability, are high surface area, large pore diameter and volume, moderate acid strength and good distribution of Brønsted and Lewis acid sites [24]. To induce moderate or high acidity, the framework structure must be modified with the inclusion of metals, such as V, Al or Fe [25–28]. The

incorporation of these metals into the MCM-41 framework also generates higher thermal and hydrothermal stability, compared to pure silica MCM-41 [29].

To understand the effects of using MCM modified by Fe or other metal as a catalyst in the ASB pyrolysis products, it is first important to understand what effect a pure silica catalyst may have on pyrolysis. In this work we analyze ASB, a lignocellulosic agro-industrial residue, as a potential feedstock to produce high added value chemicals of industrial interest. The products observed during non-catalytic and catalytic pyrolysis of ASB were monitored in the presence of different types of mesoporous silica, specifically, pure Aerosil 380 silica (Aerosil), and the one-dimensional mesoporous MCM-41. Pyrolysis products were analyzed in terms of light olefins, oxygenated compounds, furan derivatives, and aromatic compounds to study the effect of porosity and acidity on catalytic cracking, deoxygenation, and benzene, toluene, xylenes, and ethylbenzene (BTEX) production that increase the formation of chemical products of interest.

2. Results

2.1. Catalyst Characterization

The XRD pattern confirms the well-ordered hexagonal channels characteristic of MCM-41, with reflections at 2θ = 2.25 and 4.8 that correspond to the (100) and (200) planes in the MCM-41 [30–32], and a broad reflection peak of amorphous silica was observed, centered at 2θ = 23.

Figure 1a shows that the MCM-41 catalyst exhibits an isotherm type IV with a narrow hysteresis loop of type H1, characteristic of the narrow range of uniform mesoporous material, of 3.4 nm diameter [33–36]. The BJH method [37] and the approach developed by Kruk, Jaroniec, and Sayari (KJS) [38] for mesoporous materials were applied to determine the pore size distribution (Figure 1b) from desorption data. As the Table 1 shows, the MCM-41 catalyst presents a high BET surface area and a uniform pore size distribution centered at 3.4 nm.

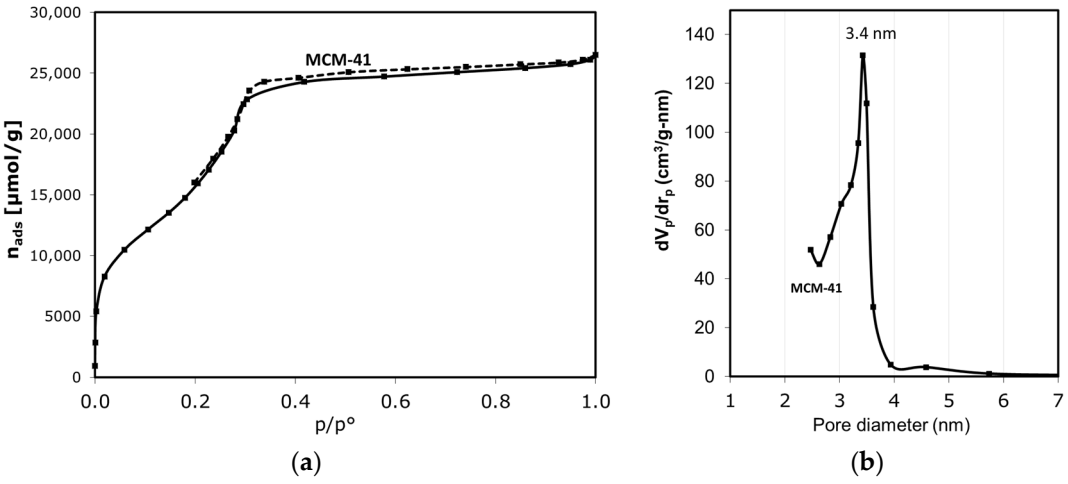

Figure 1. (**a**) Nitrogen adsorption–desorption isotherm at 77 K, and (**b**) BJH-KJS pore size distribution from desorption data, for MCM-41 catalyst.

Table 1. Textural properties of MCM-41 catalyst, obtained by nitrogen adsorption–desorption.

Catalyst	BET Surface Area (m^2/g)	Pore Diameter (nm)	Mesopore Total Volume (cm^3/g)
MCM-41	1290	3.4	0.91

FTIR spectroscopy was studied in both hydroxyl stretch (3500–3800 cm^{-1}) and fingerprint (1400–1800 cm^{-1}) regions, the latter in conjunction with pyridine adsorption

for acidity determination (Figure 2). FTIR spectra of pyridine adsorption (Figure 2b) on MCM-41 shows prominent bands at 1597 cm^{-1} and 1445 cm^{-1} associated with hydrogen-bonded (H) pyridine [39]. Yet bands corresponding to weak (L_W) and strong (L_S) Lewis acid sites (1623, 1580, and 1455 cm^{-1}) are not discernible, nor are bands related to Brønsted (B) acid sites, consistent with the lack of acidity in metal-free silica.

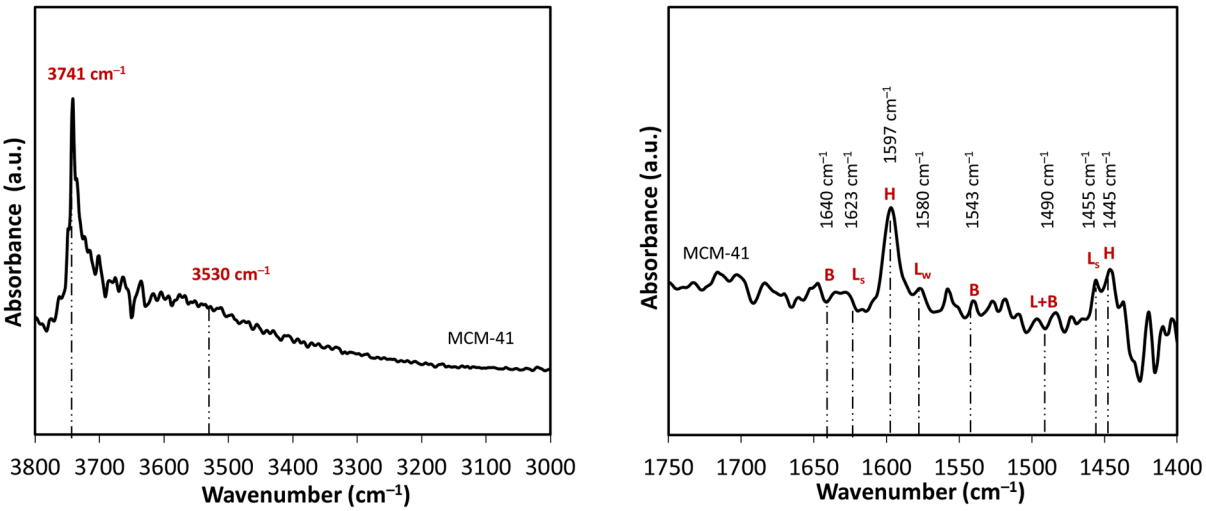

Figure 2. FTIR spectra of MCM-41 catalyst at 100 °C of (**a**) hydroxy region, and (**b**) pyridine adsorption.

2.2. Biomass Characterization

The ASB used in the pyrolysis contains less than 6 wt% moisture and low ash content (Table 2). Solids composition (Table 3) shows a high cellulose content represented by the glucose (66.5 wt%); the lignin content is close to 10 wt%. The hemicellulose is essentially xylose (20.0 wt%); other saccharides were not detected.

Table 2. Proximal analysis of the ASB.

	wt%
Moisture	5.7
Total solids	94.3
Ash	2.2

Table 3. ASB solids composition.

	wt%
Extractives	3.6
Acid insoluble lignin	9.9
Glucose	66.5
Xylose	20.0
Total	100

2.3. Thermal Decomposition of ASB by Thermogravimetric Analysis (TGA)

The thermal decomposition of the bagasse occurs in four events according to the TGA results (Figure 3). The DTG curve shows the first event occurs between 50 °C and 180 °C with a weight loss related to the evolution of water from the biomass. Weakly absorbed water is eliminated up to 120 °C, and strongly adsorbed water is eliminated at higher temperatures, as a smaller peak that ends at 180 °C. A second event appears as a shoulder in the DTG curve in the range of 180 °C to 290 °C and can be related

to hemicellulose decomposition. The maximum decomposition occurs around 255 °C according to the second derivative of the weight loss (not shown). Hemicellulose easily decomposes at low temperature due to its amorphous structure and heterogeneity [40], as it can contain xylan, mannan, xyloglucan and others saccharides in its structure, depending on the biomass sources [41]. ASB has mostly xylan which indicates that during mezcal production, hemicellulose decomposed with the loss of the other components usually found in this heteropolysaccharide. The third decomposition event occurred from 290 °C to 350 °C, appearing as an intense peak in the DTG curve with a maximum at 330 °C, and can be attributed to cellulose decomposition. Cellulose is a polysaccharide more stable than hemicellulose, since it is a linear homopolymer of glucopyranose, linked by β-1,4-glycosidic bonds, and has crystalline and amorphous zones, and its thermal decomposition is more difficult [42]. The fourth decomposition event appears as a well-defined peak from 450 °C to 490 °C in the DTG curve, with a highest decomposition rate at 470 °C, and could be related to lignin decomposition [43–47]. Lignin decomposes in a wide range of temperatures, commonly between 200 °C and 600 °C, and even higher, depending on the type of lignin.

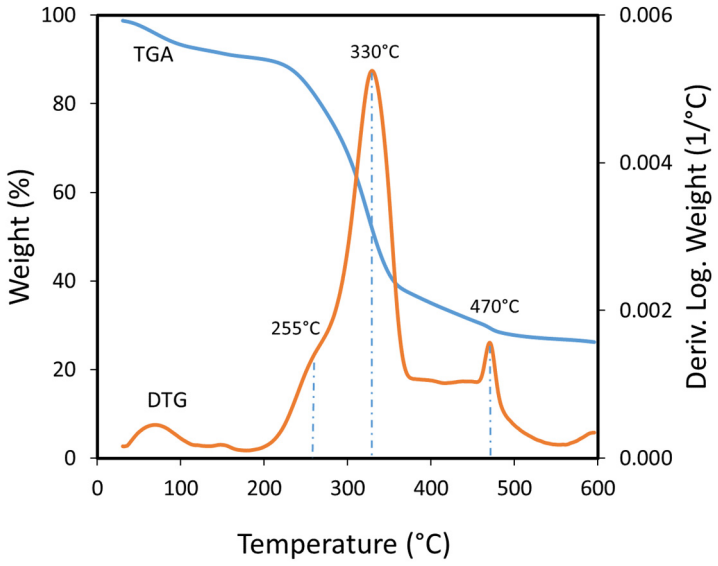

Figure 3. TGA and DTG curves obtained from *Agave salmiana* bagasse thermal decomposition.

The TGA analysis of the ASB biomass confirms the presence of three main components (hemicellulose, cellulose, and lignin) that should be considered during pyrolysis studies [45,48–50]. The overlap of the thermal decomposition of cellulose and lignin could explain the horizontal trace observed in the DTG decomposition curve from 370 °C to 460 °C, but this could be also related to the rearrangement of residues in the charring process of cellulose, and hemicellulose, principally due to the high content of minerals that could act as catalysts [51]. Finally, a shoulder that appears at the end of the DTG evidences a fifth decomposition event that occurs above 550 °C, possibly related to the production of non-condensable gases formed from the char.

2.4. Non-Catalytic Pyrolysis of Agave Salmiana Bagasse (ASB)

Using the NIST mass spectrometry database [52] as a guide it was possible to identify and follow 28 compounds, with online MS analysis, that comprise the most abundant pyrolysis products. These results appear in Figures 4–6 and show the results from room temperature to 700 °C. Figure 4a shows the production of the main non-condensable gases (CO/CO_2) and water generated during pyrolysis. The drying of the sample occurs before 200 °C in agreement with the TGA results. ASB decomposition starts at this temperature with the appearance of CO_2, with a peak at around 300 °C. This is consistent with hemicel-

lulose thermal decomposition. As reported by others, the maximum production of water and CO_2 occurs between 243 °C and 332 °C, depending on the type of hemicellulose [53]. A third event is marked by water and CO_2 emissions reaching maxima at 350 °C and 340 °C, respectively, and can be related to cellulose thermal decomposition. Additionally, a second stage of cellulose decomposition is evidenced by a shoulder at 400 °C, probably due to the presence of a more stable crystalline cellulose [54,55]. A fourth event defined by CO_2 and water emissions that start at 450 °C and reach a maximum at 485 °C is related to lignin thermal decomposition. Finally, a fifth event begins at 575 °C with maximum CO_2 production at 675 °C, corresponding to a charring and/or gasification process of residual biomass. During the last two events, there is hydrogen production with a maximum at 585 °C, in contrast to CO_2 and CO production that show a minimum at similar temperatures (575 °C).

ASB pyrolysis produces light alkanes as Figure 4b shows. Ethane is generated at a low temperature starting at 200 °C, together with water and CO_2, derived from hemicellulose thermal decomposition. The three peaks with maxima at 300 °C, 350 °C, and 485 °C indicate that ethane is produced also from cellulose and lignin. Methane, on the other hand, is mainly produced in the same temperature range where cellulose and lignin decomposed but, unlike the products already discussed, the maximum production occurs at a higher temperature (500 °C) as Figure 4b shows. Cellulose and lignin thermal decomposition also produce smaller amounts of pentane.

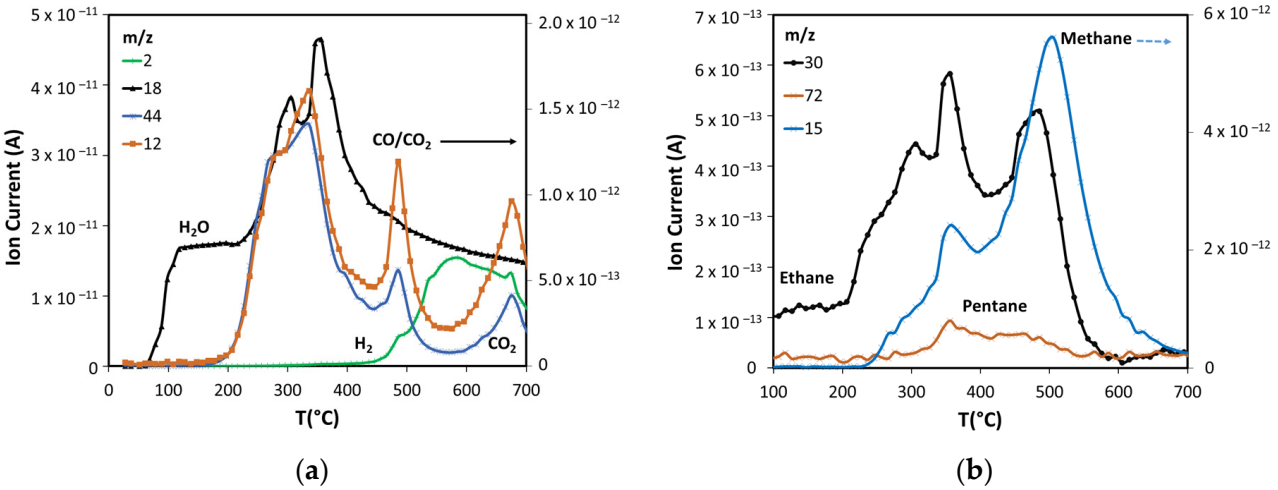

Figure 4. Products formed in non-catalytic pyrolysis of ASB. (**a**) Inorganic compounds. (**b**) Light alkanes.

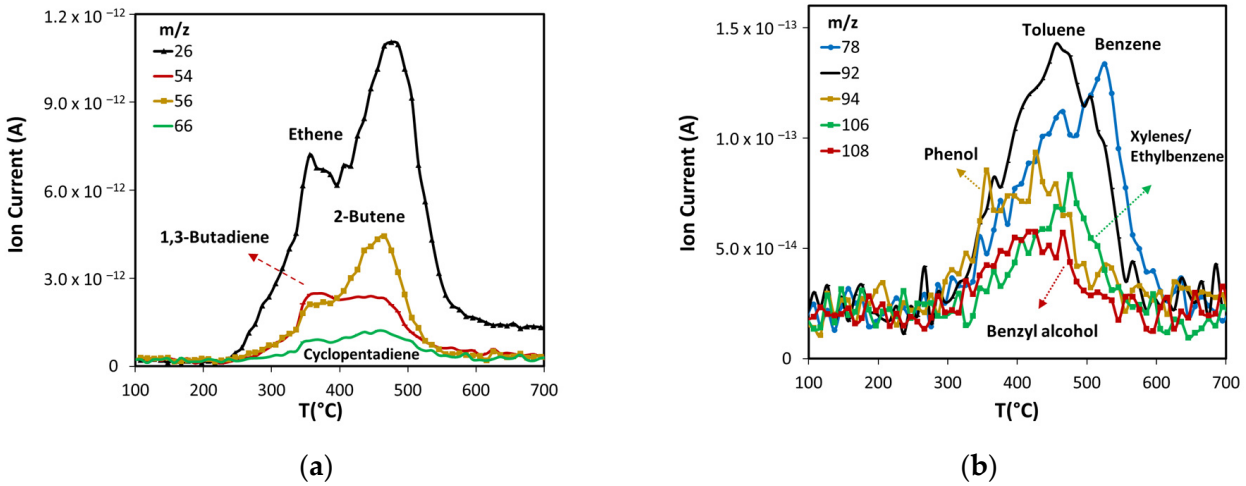

Figure 5. Products formed in non-catalytic pyrolysis of ASB. (**a**) Light olefins, and (**b**) aromatic compounds.

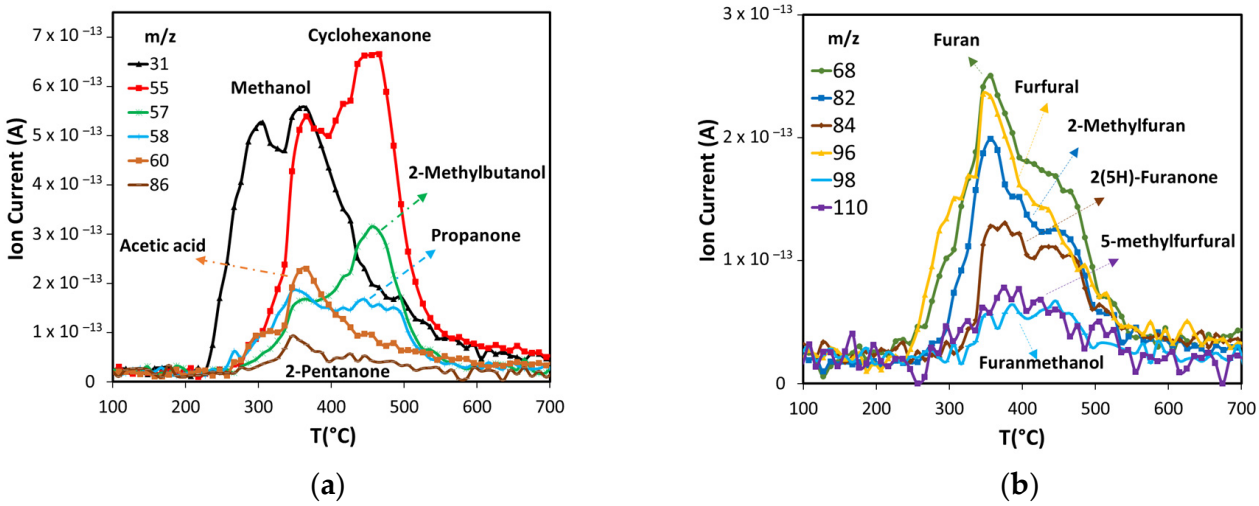

Figure 6. Products production in non-catalytic pyrolysis of ASB. (**a**) Oxygenated compounds, and (**b**) furan derivatives.

Light olefins are produced mainly from cellulose and lignin thermal decomposition. The maximum production of ethene, 2-butene, and cyclopentadiene occurs close to 475 °C (see Figure 5a), suggesting that they are produced mostly from lignin, while the 1,3-butadiene peak with a maximum at 350 °C implies it is produced principally from cellulose, but also from lignin.

The production of monoaromatic hydrocarbons during ASB thermal decomposition is related mostly to lignin decomposition (see Figure 5b). The maximum production of BETX occurs above 450 °C, namely, 455 °C for toluene, 475 °C for xylenes/ethylbenzene, and 525 °C for benzene. Toluene and benzene have maxima between 350 °C and 600 °C. Both components have peaks that coincide at 455 °C, where maximum toluene emission occurs. The production of oxygenated aromatic compounds (phenol and benzyl alcohol) occurs within the same temperature range, starting at 300 °C and ending at 600 °C.

Other volatile compounds formed during the pyrolysis include ketones, alcohols, acetic acid (Figure 6a) and furan derivatives (Figure 6b). Methanol is produced at low temperature, starting at 235 °C, and its production shows two peaks with maxima at 300 °C and 355 °C. The first is related to hemicellulose decomposition, and the second to lignin decomposition, in agreement with observations from other researchers [56,57]. Several ketones produced by cellulose and lignin thermal decomposition were detected: 2-pentanone, cyclohexanone, and propanone. Two of these ketones, cyclohexanone, and propanone, along with 2-methylbutanol, have the major production after 400 °C, with the maximum near 455 °C. This occurs when cellulose is already decomposed, thus the most likely source of these compounds is lignin, in agreement with other works [58,59]. The maximum production of acetic acid and 2-pentanone occur in the same range of temperatures as the first peak of cyclohexanone and the second of methanol. Acetic acid is produced from the carbonylation of methanol produced from hemicellulose and the carbon monoxide produced from hemicellulose and cellulose [60].

The group of furan and its derivatives (Figure 6b) have curves that show a marked high production at 355 °C due to cellulose decomposition, followed by lower production from lignin decomposition up to 450 °C.

In summary, *Agave salmiana* bagasse produces components consistent with a high cellulose and lignin content. Therefore, it has the potential to produce from pyrolysis a wide variety of chemical compounds of industrial importance. Light olefins (ethene, 2-butene, 1,3-butadiene) and BTEX are important primary building blocks of the current chemical industry. Furans (furan, furfural, 2-methylfuran, and 2(5H)-furanone) are considered as platform molecules to produce biofuel and building blocks in organic synthesis. The

oxygenated compounds (methanol, cyclohexanone, 2-methylbutanol) are of industrial importance as solvents or as feedstocks to produce other chemicals.

2.5. Use of Catalysts in Bio-Oil Upgrading

One objective of using a catalyst in pyrolysis is to reduce the oxygen content in the bio-oil through reactions of dehydration, decarboxylation, and decarbonylation. The catalyst should be able to reduce the formation of compounds with large O/C ratio. The most abundant compounds produced during ASB pyrolysis are listed in Table 4 with their respective O/C ratio and boiling points. The compounds will form part of the pyrolysis oil if their boiling point is above 50 °C, the condensate temperature that could be achieved with a large-scale condenser of pyrolysis products [61]. Of these compounds, methanol and acetic acid have the highest O/C ratios, and the lowest are cyclohexanone and benzyl alcohol. Of these, it will be desirable to eliminate or reduce the formation of acetic acid to reduce the acidity of the bio-oil. Furfural has a high O/C ratio, but it is a valuable compound that could be separated by distillation, with the possibility of having other high boiling point compounds, such as phenol and furanone, as separate products since they also have valuable applications in the industry. Finally, a desirable catalyst could be one that increases BTEX yield to obtain a bio-oil that has higher octane number and lower O/C ratio.

Table 4. Most abundant compounds identified from pyrolysis of *Agave salmiana* bagasse by mass spectrometry.

Compound	Formula	O/C Ratio	T_{bp}, °C
Bio-gas components			
Hydrogen	H_2	-	−252.9
Carbon monoxide	CO	1	−191.5
Methane	CH_4	0	−161.6
Ethene	C_2H_4	0	−103.7
Ethane	C_2H_6	0	−89
Carbon dioxide	CO_2	2	−78.5
1,3-Butadiene	C_4H_6	0	−4.4
2-Butene	C_4H_8	0	1
Furan	C_4H_4O	1/4	31
Pentane	C_5H_{12}	0	36.1
Cyclopentadiene	C_5H_6	0	40.8
Bio-oil components			
Propanone	C_3H_6O	1/3	56
2-Methylfuran	C_5H_6O	1/5	63
Methanol	CH_3OH	1	65
Benzene	C_6H_6	0	80
Water	H_2O	-	100
2-Pentanone	$C_5H_{10}O$	1/5	101
Toluene	C_7H_8	0	111
Acetic acid	CH_3COOH	1	118
2-Methylbutanol	$C_5H_{12}O$	1/5	129
Xylenes (o, m, p)/Ethylbenzene	C_8H_{10}	0	136–144
Cyclohexanone	$C_6H_{10}O$	1/6	155
Furfural	$C_5H_4O_2$	2/5	162
Furanmethanol	$C_5H_6O_2$	2/5	170
Phenol	C_6H_6O	1/6	182
5-Methylfurfural	$C_6H_6O_2$	1/3	187
Benzyl alcohol	C_7H_8O	1/7	205
2(5H)-Furanone	$C_4H_4O_2$	1/2	212

2.6. Catalytic Pyrolysis of Agave salmiana Bagasse with Aerosil

To understand the effects of using MCM-41 as a catalyst or catalyst support in the ASB pyrolysis products, it is first important to understand what effect a pure silica catalyst may have on pyrolysis. Figures 7–12 show the production curves of pyrolysis products that showed notable changes (Table 4) when Aerosil or MCM-41 were present. The use of Aerosil results in lower production of all the monitored compounds between 200 °C and 400 °C. At higher temperature, the effect of Aerosil depends on the compound type and the reactions involved in their formation.

There is little or no change in the formation pattern of carbon dioxide over the entire temperature range under study (Figure 7a), indicating that decarboxylation reactions of the polysaccharides are not affected by the presence of the Aerosil, since they occur in the bulk of the biomass. However, this is not the case for the products of other reactions, such as dehydrations.

Dehydration reactions should be favored due to the interaction between OH groups of reactant and product molecules with the silica surface [62]; however, with Aerosil, there is an overall reduction in the formation of dehydration products that include furfural, furan and its derivatives, and acetic acid (Figures 7b and 8). The formation of acetic acid occurs from hemicellulose, cellulose, and lignin, and requires the dehydration of hydroxyacetaldehyde, product of their thermal fragmentation, followed by hydration of the produced ketene to acetic acid [63]. The Aerosil surface affects both processes, with the consequent reduction of acetic acid production over the entire temperature range. Furfural is a dehydration product of glucose, the cellulose monosaccharide, and furan and its derivatives are produced from 3-deoxy-D-hexosulose, the initial dehydration product of the hexoses [64]. The rate of diffusion of the precursors increases at higher temperatures, shifting the maximum production of furan and its derivatives from 355 °C, observed in the non-catalytic ASB pyrolysis, to 450 °C with Aerosil. Although the production of these compounds above 400 °C is slightly higher than the observed values without Aerosil, their total production during pyrolysis is lower.

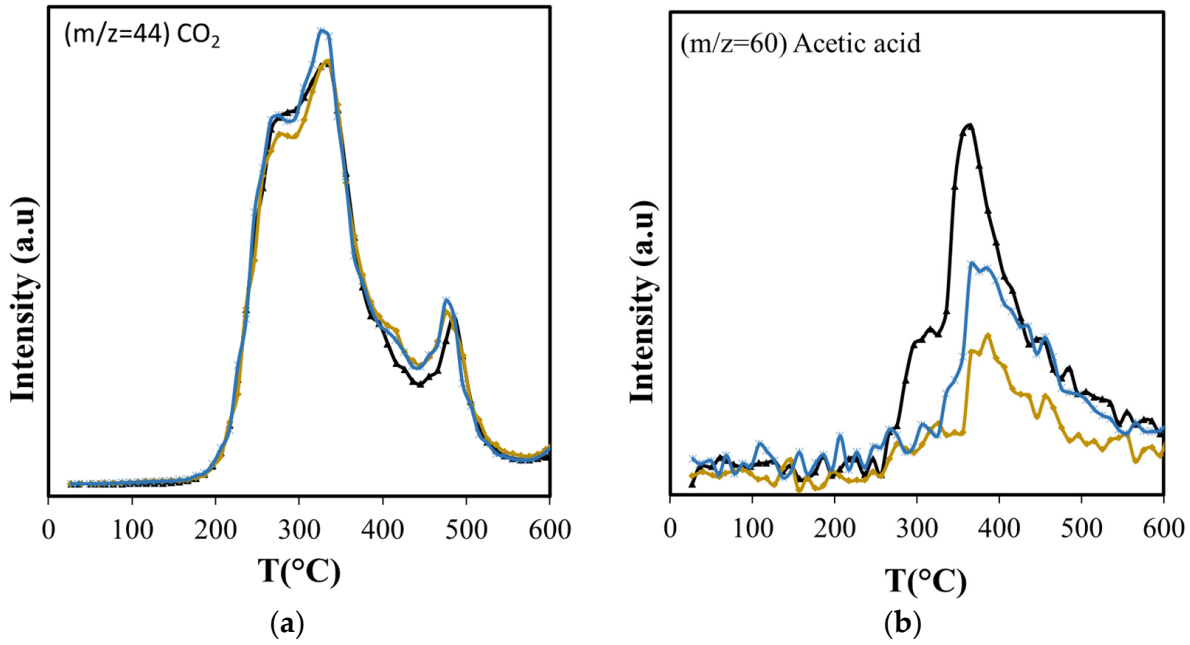

Figure 7. Effect of amorphous silica with non-structured pores (Aerosil) and with structured mesopores (MCM-41) over the production of: (**a**) CO_2 and (**b**) acetic acid. (ASB, Aerosil 380, MCM-41).

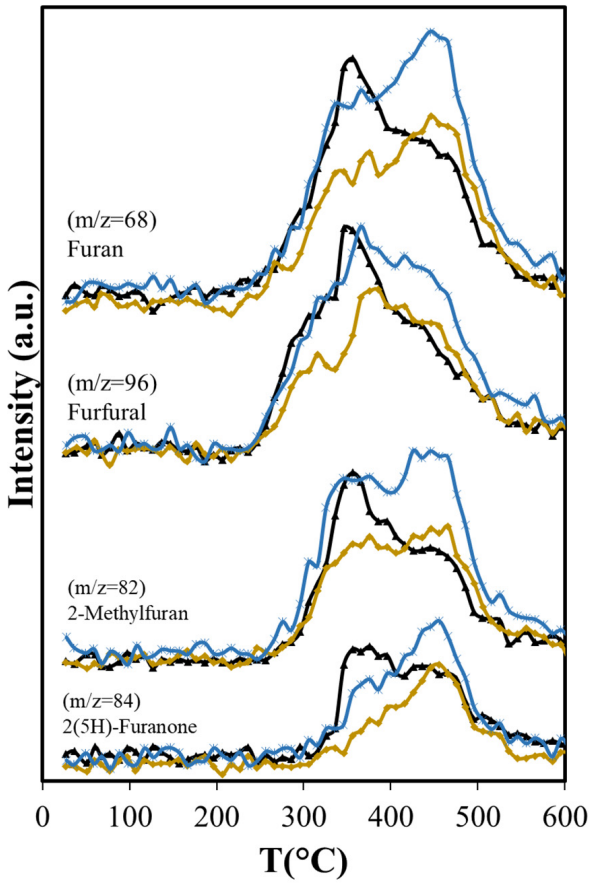

Figure 8. Effects of Aerosil 380 and MCM-41 over furan derivatives produced in catalytic pyrolysis of *Agave salmiana* bagasse. (ASB, Aerosil 380, MCM-41).

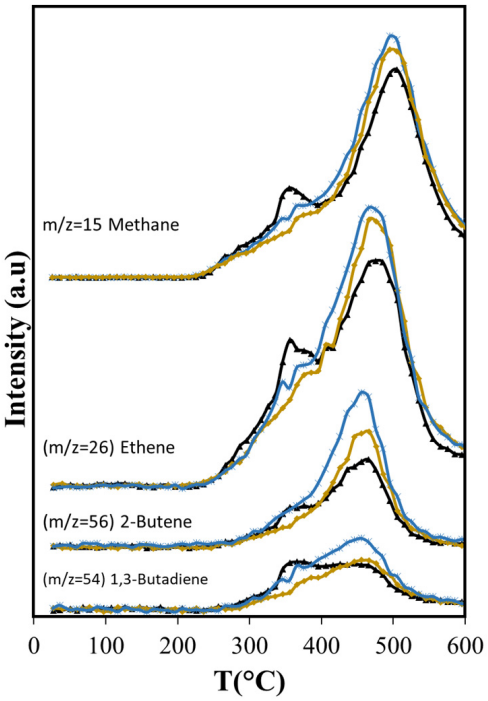

Figure 9. Effects of Aerosil 380 and MCM-41 over methane and light olefins produced in catalytic pyrolysis of *Agave salmiana* bagasse. (ASB, Aerosil 380, MCM-41).

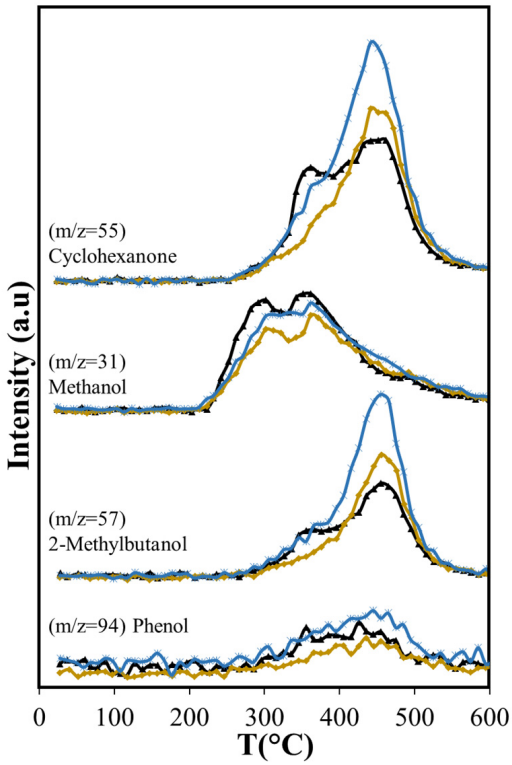

Figure 10. Effects of Aerosil 380 and MCM-41 over oxygenated compounds produced in catalytic pyrolysis of *Agave salmiana* bagasse. (ASB, Aerosil 380, MCM-41).

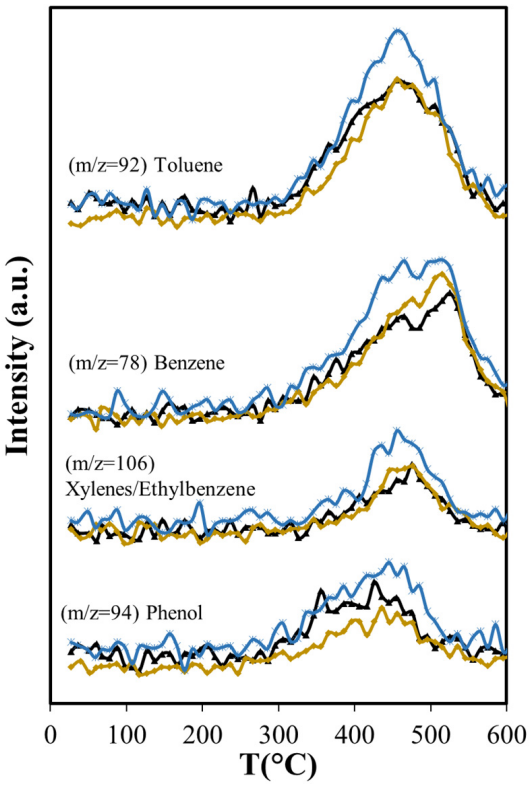

Figure 11. Effects of Aerosil 380 silica and MCM-41 over aromatic compounds produced in catalytic pyrolysis of *Agave salmiana* bagasse. (ASB, Aerosil 380, MCM-41).

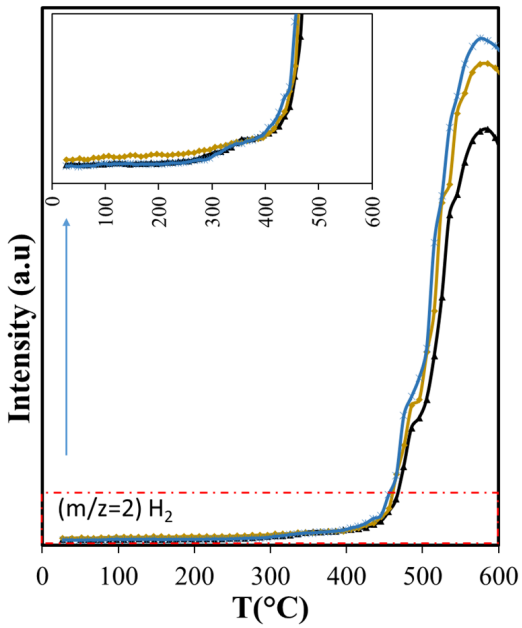

Figure 12. Effects of Aerosil and the presence of structured mesopores (MCM-41) over H_2 production. (ASB, Aerosil 380, MCM-41).

The diminished production of acetic acid results also in less production of methane before 400 °C (Figure 9) that coincides with slightly lower production of CO_2 (Figure 7a). Both compounds are the deoxygenation products of acetic acid through decarboxylation [65]. The higher production of the olefins (Figure 9) points also to increased residence times through the silica bed of the larger molecules that produce them, giving opportunity for other reactions to occur. Furans, for example, can undergo decarboxylation and decarbonylation for the production of olefins [66], yielding a larger production above 400 °C with Aerosil. Overall, the total production of methane and the olefins does not change: the lower production observed below 400 °C is compensated by the larger production that occurs at higher temperatures. Something similar occurs with 2-methylbutanol. In contrast, the overall cyclohexanone production is diminished (Figure 10). The decreased production of cyclohexanone is a consequence of lower phenol formation (Figure 10), since cyclohexanone forms from phenol hydrogenation [65]. Even when hydrogen is observed only above 450 °C, other possible sources of hydrogen at lower temperatures are formic acid and methanol.

Phenol production for T > 450 °C is not affected by Aerosil, contrasting with the lowered phenol production observed below this temperature, where cellulose and lignocellulose decomposition occur. This suggests that at higher temperatures phenol is produced directly from the thermal decomposition of the lignin. Other researchers have found during cellulose and lignocellulose pyrolysis that aromatic compounds may be formed in secondary reactions that occur in the gas phase and involve olefins. Unlike phenol, the production of benzene is higher (Figure 11) over Aerosil. In homogeneous phase experiments, benzene forms also from olefins [67] and its increased production in pyrolysis above 450 °C is the result of a higher formation of several olefins (ethene and butene), whose aromatization probably is favored in the confined space of the silica pores. The influence of Aerosil in the formation of other aromatic compounds is minimal.

2.7. Catalytic Pyrolysis of Agave salmiana Bagasse with MCM-41

We compared the pyrolysis products over non-structured pure amorphous silica (Aerosil) with a structured silica (MCM-41) to study the effect of a unidimensional hexagonal pore structure. As with the Aerosil, decarboxylation reactions are not influenced by the presence of MCM-41; consequently, the CO_2 production is very close to that observed with

non-catalytic ASB pyrolysis (Figure 7a). The effect of MCM-41 in dehydration reactions depends on the size of the molecule produced. For small molecules such as acetic acid, the production is as with Aerosil, and lower than with the non-catalytic process (Figure 7b). That is not the case for other dehydration products. Furfural, furan and its derivatives show significantly higher production using the MCM-41 than with Aerosil, and their overall production is higher than in non-catalytic pyrolysis (Figure 8 and Table 5). The unidimensional pores of the MCM-41 hinder the diffusion of large molecules, since the pore diameter of MCM-41 (3.4 nm) is smaller than the average pore size reported for Aerosil (>14.4 nm) [68]. One would expect a higher degree of interactions between the surface and the OH groups in reactants and products on the MCM-41 compared with Aerosil, due to its larger surface area (1290 vs. 380 m^2/g). A slower diffusion of molecules within the unidimensional pore structure increases the residence time of reactants in the MCM-41 catalyst bed, making them more susceptible of undergoing dehydration. Iliopoulou et al. [63] observed an increment of water produced in pyrolysis of a commercial wood biomass with the use of MCM-41 (Lignocel HBS 150-500) as catalyst and attributed this result to enhanced dehydration of the biomass pyrolysis products inside the MCM-41 tubular pores. Similar results were reported by Casoni et al. [64] in the catalytic pyrolysis of cellulose using MCM-41, in which the dehydration products yield increased. They simply attribute this to free diffusion inside the pores of molecules obtained from the primary thermal decomposition and their conversion to dehydration products; however, we believe that the increment is due to increased extent of interactions with the surface and in residence time. After all, diffusion should be facilitated in the larger pore Aerosil material, yet dehydration is inhibited. The degree of interaction with the surface is, thus, a predominant factor in the dehydration with MCM-41.

The longer residence time results in more production of olefins (ethene, butene, butadiene) (Figure 9) than with Aerosil or the non-catalytic pyrolysis, and aromatization of these molecules is favored in the confined space that MCM-41 provides, as other researchers have found with MCM-22 [69,70]. The larger production of ethylbenzene is also favored by the structure of the MCM-41, in agreement with results reported by others, showing that the alkylation of benzene with ethene occurs in other MCMs at higher conversion levels [71]. BTEX production increases 19% relative to MCM-41, while with Aerosil, the xylenes and the ethylbenzene are slightly reduced (−2.2%) and the benzene production only slightly increases (8.4%) as shown in Table 5.

The oxygen-containing molecules (cyclohexanone, 2-metyl-butanol) are also produced in larger amounts with the use of MCM-41 than with SiO_2 or in catalyst-free pyrolysis (Table 5). The increase in cyclohexanone and 2-methyl-butanol production coincides exactly with the maximum in phenol production. The temperature at which maximum production occurs does not change with the presence of the catalysts, but the amount evolved does, increasing significantly with the presence of MCM-41. These compounds are derived from lignin, since in the temperature range where cellulose and hemicellulose decomposition occurs, their production is very low, only becoming higher when the lignin pyrolysis is the only process. The temperature range where they evolve without catalyst does not shift when catalyst is present. Importantly, the overall production of acetic acid is reduced with Aerosil and MCM-41, the reduction being more than two-fold with Aerosil (−50.7 % vs. −22.1 %). Methanol reduction is also greater with Aerosil (−16.9%) than with MCM-41 (−2.9%). This is also observed with 2(5H)-Furanone, showing a large reduction with Aerosil (−32.9%), while the effect of MCM-41 is practically negligible (−0.4%). This result is significant, given that acetic acid, methanol, and 2(5H)-Furanone have the highest O/C values in the bio-oil (Table 4).

In summary, the major difference in the production of the monitored compounds between the non-catalytic pyrolysis and the pyrolysis in the presence of the MCM-41 occurs at temperatures above 400 °C. Aerosil produces a less acidic bio-oil, while MCM promotes deformation of olefins, BTEX, furfural and furan derivatives.

Table 5. Increase or decrease in cumulative production of compounds due to the presence of silica catalysts during ASB pyrolysis.

Compound	Aerosil-380, %	MCM-41, %
Acetic acid	−50.7	−22.1
Methanol	−16.9	−2.9
2(5H)-Furanone	−32.9	−0.4
CO_2	1.4	3.5
Ethene	2.5	8.9
Methane	1.9	10.4
1,3-Butadiene	−14.2	15.6
Furfural	−13.8	16.6
Toluene	−1.0	17.3
Benzene	8.4	19.6
Furan	−16.9	23.7
Phenol	−6.8	27.3
Xylenes/Ethylbenzene	−2.2	27.4
H_2	10.1	28.7
Cyclohexanone	−15.9	37.9
2-Methylfuran	−4.6	40.4
2-Methylbutanol	−2.0	42.5
2-butene	6.3	44.6

3. Materials and Methods

3.1. Biomass Preparation and Characterization

The *Agave salmiana* bagasse (ASB) was provided by the distillery Ipiña located in San Luis Potosí (México). The bagasse is the residue generated after the agave's core is baked and the juice is extracted. The biomass was dried in a stove to have 3% of moisture, milled in a commercial blender and sieved to obtain a particle size smaller than 0.297 mm. The biomass thermal decomposition was studied with a TA Instruments Q500 TGA (New Castle, DE, USA) thermogravimetric analyzer.

Moisture content, total solids, and ash in the ASB were determined following the methodology described by the National Renewable Energy Laboratory (NREL) [72,73]. About 2 g of ASB were dried at 110 °C for 4 h to determine the moisture and the total solids. The analysis was triplicated. For ash determination, 0.5 g of ASB previously dried at 110 °C were calcined in a tube furnace (Lindberg/Blue M, Thermo Scientific, Waltham, MA, USA) under air with a 75 mL/min flowrate at 575 °C for 3 h. Extractives in hot water and structural carbohydrates were determined following the Laboratory Analytical Procedure described by the NREL [74,75]. For this, 5 g of ASB previously dried at 110 °C were subjected to extraction for 2 h at 60 °C. Structural carbohydrates were determined by applying a two-step hydrolysis to 0.3 g of previously dried ASB, using 3 mL of 72% sulfuric acid, and held at 30 °C for 1 h with stirring applied in 5–10 min intervals. The acid was then diluted to 4% by adding 84 mL of MQ water. The contents were then heated and held at 115 °C for 3 h, together with sugar recovery standards for glucose, xylose, galactose, arabinose, and mannose for correction due to sugar losses. Once the hydrolysis was completed, the mixture was filtered and the neutralized liquor analyzed by HPLC (Shimadzu, Kyoto, Japan) for sugars determination using an Aminex 87H (BioRad, Hercules, CA. USA) column at pH 2, 0.6 mL/min, and refractive index detector. The remaining solids were dried overnight at 60 °C to determine the acid insoluble lignin.

3.2. Catalyst Synthesis

In the synthesis of MCM-41, the molar proportion of reactants used was $1SiO_2/0.65$ CTAB/0.5 NaOH/62 H_2O. Two grams of Aerosil 380 was mixed with 27 mL of water under constant stirring for 40 min at ambient conditions; 5 mL of 3.4 M NaOH solution was then added and stirred for 30 min; 7.88 g of cetyltrimethylammonium bromide (CTAB) in powder form at 99% of purity was added to the mixture and stirred for 1 h at

40 °C. The mixture obtained was aged for 24 h in an autoclave at 120 °C, and dried for 5 h at 100 °C. The product received hydrothermal treatment in an autoclave for 16 h, using a ratio of 1 g of catalyst powder for 50 mL of deionized water, and lastly washed with 100 mL of an 50% ethanol/water mixture to partially remove the CTAB while it was filtered, and dried for 8 h at 100 °C. Finally, catalyst was calcined for 8 h at 550 °C in an inert atmosphere, and 4 h with air ambient.

3.3. Scanning Electron Microscopy (SEM), and High Resolution Transmition Electron Microscopy (HR-TEM)

MCM-41 catalyst nanostructure was studied via scanning electron microscopy (SEM) performed on a Hitachi STEM-5500 (Tokyo, Japan) equipped with dark field and bright field detectors. High-resolution transmission electron microscopy (HR-TEM) was performed with a JEOL JEM 2010F Field emission electron microscope (Tokyo, Japan).

3.4. Small Angle X-ray Scattering (SAXS), and Large X-ray Diffraction (XRD)

Small angle X-ray scattering (SAXS) analysis was made in a Nanostar (Bruker, Billerica, MA, USA) instrument, and X-ray diffraction (XRD) patterns at high angle were acquired in a Rigaku (Tokyo, Japan) DMAX 2200 to perform the structural characterization of the catalysts.

3.5. Nitrogen Physisorption

N_2 physisorption isotherms were measured to determine pore size and distribution by Barret—Joyner—Halenda (BJH) method, and volume pore and surface area by the Brunauer–Emmett–Teller (BET) method. The experimental details and the equipment were previously described [76].

3.6. Fourier-Transform Infrared Spectroscopy

Pyridine was used as a probe molecule to identify the type of acid sites (Brønsted or Lewis) in the catalysts. For this purpose, the catalyst samples were placed in a diffuse-reflectance cell (Harrick "Praying Mantis", Pleasantville, NY, USA) equipped with an environmental chamber and KBr windows, mounted on a Bruker Vector 22 FTIR spectrometer (Bruker, Billerica, MA., USA). Catalysts samples were pre-treated at 300 °C in nitrogen flow (50 mL/min) for 60 min, then cooled to 100 °C. The infrared spectra of the clean sample were taken as a reference, after this 0.03 mL of pyridine were injected into the nitrogen flow, and the IR spectra was taken after 30 min of pyridine injection.

3.7. Conventional, and Catalytic Pyrolysis

Pyrolysis was conducted in a stainless-steel tubular microreactor (OD = 1/4"), coupled with a MS for product analysis by monitoring 200 m/z ratios. N_2 was used as the carrier gas at 100 mL/min flow rate, and a heating rate of 10 °C/min was used to reach the target temperature. Conventional and catalytic pyrolysis experiments used 200 mg of biomass. For catalytic pyrolysis a bed of 80 mg of catalyst was located downstream separated from the biomass bed by 20 mg of fiberglass. The loaded catalyst was previously pelletized at 500 kg/m^2 in a bench top hydraulic press and crushed to small particle size and used without sieving. At the reactor exit, higher boiling pyrolysis products were condensed in an ice cooled flask. Products formed from conventional pyrolysis of ASB were monitored from ambient temperature to 700 °C with a mass spectrometer (Pfeiffer OmniStar GSD320, Aßlar, Germany); the heater of the capillary tubing was maintained at 300 °C to prevent vapors condensation.

4. Conclusions

The *Agave salmiana* bagasse has a great potential to be used as a feedstock in the production of a wide variety of compounds, such as olefins, furan derivatives, aromatics, and some oxygenated compounds of interest, namely, cyclohexanone and phenol. Through

catalytic pyrolysis at temperatures above 400 °C, and the use of mesoporous materials such as MCM-41, this can significantly change the products distribution, improving the deoxygenation process and promoting the cracking of larger fragments originated in the biomass pyrolysis, reducing the methanol and acid acetic content, and increasing desired products, such as ethene, 2-butene, 1,3-butadiene, 2-methylbutanol, furan, 2-methylfuran, toluene, and benzene, among others. The studies with Aerosil showed a lower production of dehydration products, yet reactions that occur in the biomass bulk, such as decarboxylation and formation of phenol from lignin, are unaffected.

The use of mesoporous catalysts with a large surface area, such as MCM-41, do not affect decarboxylation reactions but do promote dehydration and olefins aromatization, given there is sufficient access of the fragment molecules produced during biomass pyrolysis to the unidimensional pore structure. Consequently, pyrolysis processes based on the use of these catalysts could produce a bio-oil that is less corrosive because of the anticipated lower acid content, as well as better quality as a fuel due to increased BTEX content and decreased oxygen content. In addition, the increase in production of furfural, furan, and furan derivatives useful in the production of other industrially important chemicals is noteworthy.

Author Contributions: Conceptualization, M.-G.C.-G. and L.S.-M.; methodology, M.-G.C.-G., J.R.-H., B.E.H., C.I.G.-F. and L.S.-M.; validation, L.S.-M. and M.-G.C.-G.; formal analysis, L.S.-M., M.-G.C.-G. and B.E.H.; investigation, L.S.-M. and C.I.G.-F.; resources, M.-G.C.-G., J.R.-H. and B.E.H.; data curation, L.S.-M. and C.I.G.-F.; writing—original draft preparation, L.S.-M.; writing—review and editing, M.-G.C.-G. and B.E.H.; supervision, M.-G.C.-G.; project administration, M.-G.C.-G.; funding acquisition, M.-G.C.-G. All authors have read and agreed to the published version of the manuscript.

Funding: Financial support from CONACyT with the postgraduate fellowship number 442317, research funding with the project CB-255527-2016. Financial support from UASLP through the project C17-FRC-04-08.08.

Data Availability Statement: All data are provided within the article.

Acknowledgments: The authors acknowledge the assistance of Yadira Elena Marin Proa and Araceli Juárez Martínez for their technical support, the assistance of Hoya Ihara in the use of HPLC for sugars quantification.

Conflicts of Interest: The authors declare no conflict of interest.

References

1. Alonso, D.M.; Bond, J.Q.; Dumesic, J.A. Catalytic conversion of biomass to biofuels. *Green Chem.* **2010**, *12*, 1493–1513. [CrossRef]
2. Huber, G.W.; Iborra, S.; Corma, A. Synthesis of transportation fuels from biomass: Chemistry, catalysts, and engineering. *Chem. Rev.* **2006**, *106*, 4044–4098. [CrossRef] [PubMed]
3. Zhang, Y.H.P. Reviving the carbohydrate economy via multi-product lignocellulose biorefineries. *J. Ind. Microbiol. Biotechnol.* **2008**, *35*, 367–375. [CrossRef]
4. Cushman, J.C.; Davis, S.C.; Yang, X.; Borland, A.M. Development and use of bioenergy feedstocks for semi-arid and arid lands. *J. Exp. Bot.* **2015**, *66*, 4177–4193. [CrossRef] [PubMed]
5. Nava-Cruza, N.Y.; Medina-Moralesa, M.A.; Martineza, J.L.; Rodrigueza, R.; Aguilara, C.N. Agave biotechnology: An overview. *Crit. Rev. Biotechnol.* **2015**, *35*, 546–559. [CrossRef] [PubMed]
6. Davis, S.C.; Dohleman, F.G.; Long, S.P. The global potential for Agave as a biofuel feedstock. *GCB Bioenergy* **2011**, *3*, 68–78. [CrossRef]
7. Hoz-Zavala, M.E.E.; Nava-Diguero, P. Situación del Agave y sus residuos en Tamaulipas. *Rev. Energías Renov.* **2017**, *1*, 19–31.
8. Chávez-Guerrero, L.; Hinojosa, M. Bagasse from the mezcal industry as an alternative renewable energy produced in arid lands. *Fuel* **2010**, *89*, 4049–4052. [CrossRef]
9. Consejo Regulador del Tequila Informe Estadístico del Consejo Regulador del Tequila. 2021. Available online: https://www.crt.org.mx/EstadisticasCRTweb/. (accessed on 11 March 2022).
10. Consejo Regulador del Mezcal Información Estadístico 2020. Available online: http://www.crm.org.mx/informes.php (accessed on 30 March 2021).
11. Hoz-Zavala, M.E.E.; Nava-Diguero, P. Los residuos de agave como factor de corrosión del suelo donde se vierte. *Rev. Desarro. Tecnol.* **2017**, *1*, 11–24.

12. Jiménez Muñoz, E.; Prieto García, F.; Prieto Méndez, J.; Acevedo Sandoval, O.A.; Rodríguez Laguna, R.; Otazo Sánchez, E.M. Utilization of Waste Agaves: Potential for Obtaining Cellulose Pulp. *Cienc. Tec. Vitivinic.* **2014**, *29*, 223–254.
13. Pinos-Rodríguez, J.M.; Aguirre-Rivera, J.R.; García-López, J.C.; Rivera-Miranda, M.T.; González-Muñoz, S.; López-Aguirre, S.; Chávez-Villalobos, D. Use of "maguey" (*Agave salmiana* otto ex. salm-dick) as forage for ewes. *J. Appl. Anim. Res.* **2006**, *30*, 101–107. [CrossRef]
14. Parascanu, M.M.; Sandoval-Salas, F.; Soreanu, G.; Valverde, J.L.; Sanchez-Silva, L. Valorization of Mexican biomasses through pyrolysis, combustion and gasification processes. *Renew. Sustain. Energy Rev.* **2017**, *71*, 509–522. [CrossRef]
15. Saucedo-Luna, J.; Castro-Montoya, A.J.; Rico, J.L.; Campos-García, J. Optimización de hidrólisis ácida de bagaso de Agave tequilana Weber. *Rev. Mex. Ing. Qum.* **2010**, *9*, 91–97.
16. Liñán-Montes, A.; De La Parra-Arciniega, S.M.; Garza-González, M.T.; García-Reyes, R.B.; Soto-Regalado, E.; Cerino-Córdova, F.J. Characterization and thermal analysis of agave bagasse and malt spent grain. *J. Therm. Anal. Calorim.* **2014**, *115*, 751–758. [CrossRef]
17. Bernardo, G.R.R.; Rene, R.M.J. Contribution of agro-waste material main components (hemicelluloses, cellulose, and lignin) to the removal of chromium (III) from aqueous solution. *J. Chem. Technol. Biotechnol.* **2009**, *84*, 1533–1538. [CrossRef]
18. Akhtar, J.; Saidina Amin, N. A review on operating parameters for optimum liquid oil yield in biomass pyrolysis. *Renew. Sustain. Energy Rev.* **2012**, *16*, 5101–5109. [CrossRef]
19. Torres, C.; Rostom, S.; de Lasa, H. An Eco-Friendly Fluidizable FexOy/CaO-γ-Al_2O_3 Catalyst for Tar Cracking during Biomass Gasification Cindy. *Catalysts* **2020**, *10*, 806. [CrossRef]
20. Li, P.; Li, D.; Yang, H.; Wang, X.; Chen, H. Effects of Fe-, Zr-, and Co-Modified Zeolites and Pretreatments on Catalytic Upgrading of Biomass Fast Pyrolysis Vapors. *Energy Fuels* **2016**, *30*, 3004–3013. [CrossRef]
21. Kelkar, S.; Saffron, C.M.; Andreassi, K.; Li, Z.; Murkute, A.; Miller, D.J.; Pinnavaia, T.J.; Kriegel, R.M. A survey of catalysts for aromatics from fast pyrolysis of biomass. *Appl. Catal. B Environ.* **2015**, *174–175*, 85–95. [CrossRef]
22. Xue, Z.; Zhong, Z.; Zhang, B. Microwave-assisted catalytic fast pyrolysis of biomass for hydrocarbon production with physically mixed MCM-41 and ZSM-5. *Catalysts* **2020**, *10*, 685. [CrossRef]
23. Ratnasari, D.K.; Bijl, A.; Yang, W.; Jönsson, P.G. Effect of H-ZSM-5 and Al-MCM-41 proportions in catalyst mixtures on the composition of bio-oil in ex-situ catalytic pyrolysis of lignocellulose biomass. *Catalysts* **2020**, *10*, 868. [CrossRef]
24. De, S.; Dutta, S.; Saha, B. Critical design of heterogeneous catalysts for biomass valorization: Current thrust and emerging prospects. *Catal. Sci. Technol.* **2016**, *6*, 7364–7385. [CrossRef]
25. Diez, A.S.; Alvarez, M.; Volpe, M.A. Metal-modified mesoporous silicate (MCM-41) material: Preparation, characterization and applications as an adsorbent. *J. Braz. Chem. Soc.* **2015**, *26*, 1542–1550. [CrossRef]
26. Taguchi, A.; Schüth, F. Ordered mesoporous materials in catalysis. *Microporous Mesoporous Mater.* **2005**, *77*, 1–45. [CrossRef]
27. Meziani, M.J.; Zajac, J.; Jones, D.J.; Partyka, S.; Rozière, J.; Auroux, A. Number and strength of surface acidic sites on porous aluminosilicates of the MCM-41 type inferred from a combined microcalorimetric and adsorption study. *Langmuir* **2000**, *16*, 2262–2268. [CrossRef]
28. Martín-Aranda, R.M.; Čejka, J. Recent advances in catalysis over mesoporous molecular sieves. *Top. Catal.* **2010**, *53*, 141–153. [CrossRef]
29. Carrott, M.M.L.R.; Este, A.J.; Carrott, P.J.M.; Unger, K.K. Evaluation of the Stability of Pure Silica MCM-41 toward Water Vapor. *Langmuir* **1999**, *15*, 8895–8901. [CrossRef]
30. Hu, S.; Liu, D.; Li, L.; Borgna, A.; Yang, Y. A non-sodium synthesis of highly ordered V-MCM-41 and its catalytic application in isomerization. *Catal. Lett.* **2009**, *129*, 478–485. [CrossRef]
31. Wang, X.; Zhou, G.; Chen, Z.; Jiang, W.; Zhou, H. In-situ synthesis and characterization of V-MCM-41 for oxidative dehydrogenation of n-butane. *Microporous Mesoporous Mater.* **2016**, *223*, 261–267. [CrossRef]
32. Beck, J.S.; Vartuli, J.C.; Roth, W.J.; Leonowicz, M.E.; Kresge, C.T.; Schmitt, K.D.; Chu, C.T.W.; Olson, D.H.; Sheppard, E.W.; McCullen, S.B.; et al. A New Family of Mesoporous Molecular Sieves Prepared with Liquid Crystal Templates. *J. Am. Chem. Soc.* **1992**, *114*, 10834–10843. [CrossRef]
33. Thommes, M.; Kaneko, K.; Neimark, A.V.; Olivier, J.P.; Rodriguez-Reinoso, F.; Rouquerol, J.; Sing, K.S.W. Physisorption of gases, with special reference to the evaluation of surface area and pore size distribution (IUPAC Technical Report). *Pure Appl. Chem.* **2015**, *87*, 1051–1069. [CrossRef]
34. Kresge, C.T.; Leonowicz, M.E.; Roth, W.J.; Vartuli, J.C.; Beck, J.S. Ordered mesoporous molecular sieves synthesized by a liquid-crystal template mechanism. *Nature* **1992**, *359*, 710–712. [CrossRef]
35. Amama, P.B.; Lim, S.; Ciuparu, D.; Yang, Y.; Pfefferle, L.; Haller, G.L. Synthesis, characterization, and stability of Fe-MCM-41 for production of carbon nanotubes by acetylene pyrolysis. *J. Phys. Chem. B* **2005**, *109*, 2645–2656. [CrossRef] [PubMed]
36. Froba, M.; Thommes, M.; Ko, R. Sorption and pore condensation behavior of pure fluids in mesoporous MCM-48 silica, MCM-41 silica, SBA-15 silica and controlled-pore glass at temperatures above and below the bulk triple point. *Appl. Surf. Sci.* **2002**, *196*, 239–249.
37. Barrett, E.P.; Joyner, L.G.; Halenda, P.P. The Determination of Pore Volume and Area Distributions in Porous Substances. I. Computations from Nitrogen Isotherms. *J. Am. Chem. Soc.* **1951**, *73*, 373–380. [CrossRef]
38. Kruk, M.; Jaroniec, M.; Sayari, A. Application of Large Pore MCM-41 Molecular Sieves To Improve Pore Size Analysis Using Nitrogen Adsorption Measurements. *Langmuir* **2002**, *13*, 6267–6273. [CrossRef]

39. Chakraborty, B.; Viswanathan, B. Surface acidity of MCM-41 by in situ IR studies of pyridine adsorption. *Catal. Today* **1999**, *49*, 253–260. [CrossRef]
40. Yang, H.; Yan, R.; Chen, H.; Lee, D.H.; Zheng, C. Characteristics of hemicellulose, cellulose and lignin pyrolysis. *Fuel* **2007**, *86*, 1781–1788. [CrossRef]
41. Zhou, X.; Li, W.; Mabon, R.; Broadbelt, L.J. A Critical Review on Hemicellulose Pyrolysis. *Energy Technol.* **2017**, *5*, 216. [CrossRef]
42. Shen, D.K.; Gu, S. The mechanism for thermal decomposition of cellulose and its main products. *Bioresour. Technol.* **2009**, *100*, 6496–6504. [CrossRef] [PubMed]
43. Liu, C.; Hu, J.; Zhang, H.; Xiao, R. Thermal conversion of lignin to phenols: Relevance between chemical structure and pyrolysis behaviors. *Fuel* **2016**, *182*, 864–870. [CrossRef]
44. Monteil-Rivera, F.; Phuong, M.; Ye, M.; Halasz, A.; Hawari, J. Isolation and characterization of herbaceous lignins for applications in biomaterials. *Ind. Crops Prod.* **2013**, *41*, 356–364. [CrossRef]
45. Sanchez-Silva, L.; López-González, D.; Villaseñor, J.; Sánchez, P.; Valverde, J.L. Thermogravimetric-mass spectrometric analysis of lignocellulosic and marine biomass pyrolysis. *Bioresour. Technol.* **2012**, *109*, 163–172. [CrossRef]
46. Shen, D.K.; Gu, S.; Luo, K.H.; Wang, S.R.; Fang, M.X. The pyrolytic degradation of wood-derived lignin from pulping process. *Bioresour. Technol.* **2010**, *101*, 6136–6146. [CrossRef]
47. Wang, S.; Wang, K.; Liu, Q.; Gu, Y.; Luo, Z.; Cen, K.; Fransson, T. Comparison of the pyrolysis behavior of lignins from different tree species. *Biotechnol. Adv.* **2009**, *27*, 562–567. [CrossRef] [PubMed]
48. Shen, D.; Jin, W.; Hu, J.; Xiao, R.; Luo, K. An overview on fast pyrolysis of the main constituents in lignocellulosic biomass to valued-added chemicals: Structures, pathways and interactions. *Renew. Sustain. Energy Rev.* **2015**, *51*, 761–774. [CrossRef]
49. Stefanidis, S.D.; Kalogiannis, K.G.; Iliopoulou, E.F.; Michailof, C.M.; Pilavachi, P.A.; Lappas, A.A. A study of lignocellulosic biomass pyrolysis via the pyrolysis of cellulose, hemicellulose and lignin. *J. Anal. Appl. Pyrolysis* **2014**, *105*, 143–150. [CrossRef]
50. Wu, S.; Shen, D.; Hu, J.; Zhang, H.; Xiao, R. Cellulose-lignin interactions during fast pyrolysis with different temperatures and mixing methods. *Biomass Bioenergy* **2016**, *90*, 209–217. [CrossRef]
51. Collard, F.X.; Blin, J. A review on pyrolysis of biomass constituents: Mechanisms and composition of the products obtained from the conversion of cellulose, hemicelluloses and lignin. *Renew. Sustain. Energy Rev.* **2014**, *38*, 594–608. [CrossRef]
52. Acree, W.E.; Chickos, J.J.S. Mass pectra. In *NIST Chemistry WebBook Standar Reference Database Number 69*; Linstrom, P.J., Mallard, W.G., Eds.; National Institute of Standars and Technology: Gaithersburg, MD, USA, 2005.
53. Werner, K.; Pommer, L.; Broström, M. Thermal decomposition of hemicelluloses. *J. Anal. Appl. Pyrolysis* **2014**, *110*, 130–137. [CrossRef]
54. Wang, Z.; McDonald, A.G.; Westerhof, R.J.M.; Kersten, S.R.A.; Cuba-Torres, C.M.; Ha, S.; Pecha, B.; Garcia-Perez, M. Effect of cellulose crystallinity on the formation of a liquid intermediate and on product distribution during pyrolysis. *J. Anal. Appl. Pyrolysis* **2013**, *100*, 56–66. [CrossRef]
55. Kim, U.; Hyun, S.; Wada, M. Thermal decomposition of native cellulose: In fluence on crystallite size. *Polym. Degrad. Stab.* **2010**, *95*, 778–781. [CrossRef]
56. Degroot, W.F.; Pan, W.P.; Rahman, M.D.; Richards, G.N. First chemical events in pyrolysis of wood. *J. Anal. Appl. Pyrolysis* **1988**, *13*, 221–231. [CrossRef]
57. Yogalakshmi, K.N.; Poornima Devi, T.; Sivashanmugam, S.; Kavitha, S.; Yukesh Kannah, R.; Varjani, S.; AdishKumar, S.; Kumar, G.; Rajesh Banu, J. Lignocellulosic biomass-based pyrolysis: A comprehensive review. *Chemosphere* **2022**, *286*, 131824. [CrossRef]
58. Boot, M.; Frijters, P.; Luijten, C.; Somers, B.; Baert, R.; Donkerbroek, A.; Klein-Douwel, R.J.H.; Dam, N. Cyclic oxygenates: A new class of second-generation biofuels for diesel engines? *Energy Fuels* **2009**, *23*, 1808–1817. [CrossRef]
59. Nimmanwudipong, T.; Runnebaum, R.C.; Block, D.E.; Gates, B.C. Catalytic reactions of guaiacol: Reaction network and evidence of oxygen removal in reactions with hydrogen. *Catal. Lett.* **2011**, *141*, 779–783. [CrossRef]
60. Azeez, A.M.; Meier, D.; Odermatt, J. Temperature dependence of fast pyrolysis volatile products from European and African biomasses. *J. Anal. Appl. Pyrolysis* **2011**, *90*, 81–92. [CrossRef]
61. Papari, S.; Hawboldt, K. A review on condensing system for biomass pyrolysis process. *Fuel Process. Technol.* **2018**, *180*, 1–13. [CrossRef]
62. Barnette, A.L.; Asay, D.B.; Janik, M.J.; Kim, S.H. Adsorption isotherm and orientation of alcohols on hydrophilic SiO_2 under ambient conditions. *J. Phys. Chem. C* **2009**, *113*, 10632–10641. [CrossRef]
63. Güllü, D.; Demirbaş, A. Biomass to methanol via pyrolysis process. *Energy Convers. Manag.* **2001**, *42*, 1349–1356. [CrossRef]
64. Shafizadeh, F. Introduction to pyrolysis of biomass. *J. Anal. Appl. Pyrolysis* **1982**, *3*, 283–305. [CrossRef]
65. Samolada, M.C.; Papafotica, A.; Vasalos, I.A. Catalyst Evaluation for Catalytic Biomass Pyrolysis. *Energy Fuels* **2000**, *14*, 1161–1167. [CrossRef]
66. Vispute, T.P.; Zhang, H.; Sanna, A.; Xiao, R.; Huber, G.W. Renewable chemical commodity feedstocks from integrated catalytic processing of pyrolysis oils. *Science* **2010**, *330*, 1222–1227. [CrossRef] [PubMed]
67. Evans, R.J.; Milne, T.A. An American Chemical Society Journal. *Energy Fuels* **1987**, *1*, 123–137. [CrossRef]
68. Conner, W.C.; Weist, E.L.; Ito, T.; Fraissard, J. Characterization of the porous structure of agglomerated microspheres by129Xe NMR spectroscopy. *J. Phys. Chem.* **1989**, *93*, 4138–4142. [CrossRef]
69. Niu, X.; Song, Y.; Xie, S.; Liu, S.; Wang, Q.; Xu, L. Synthesis and catalytic reactivity of MCM-22/ZSM-35 composites for olefin aromatization. *Catal. Lett.* **2005**, *103*, 211–218. [CrossRef]

70. Kumar, N.; Lindfors, L.E. Synthesis, characterization and application of H-MCM-22, Ga-MCM-22 and Zn-MCM-22 zeolite catalysts in the aromatization of n-butane. *Appl. Catal. A Gen.* **1996**, *147*, 175–187. [CrossRef]
71. Corma, A.; Martínez-Soria, V.; Schnoeveld, E. Alkylation of benzene with short-chain olefins over MCM-22 zeolite: Catalytic behaviour and kinetic mechanism. *J. Catal.* **2000**, *192*, 163–173. [CrossRef]
72. Sluiter, A.; Hames, B.; Ruiz, R.; Scarlata, C.; Sluiter, J.; Templeton, D. *Determination of Ash in Biomass*; NREL/TP-510-42622; NREL, Laboratory Analytical Procedure (LAP): Golden, CO, USA, 2008.
73. Sluiter, A.; Hames, B.; Hyman, D.; Payne, C.; Ruiz, R.; Scarlata, C.; Sluiter, J.; Templeton, D.; Wolfe, J. *Determination of Total Solids in Biomass and Total Dissolved Solids in Liquid Process Samples*; NREL/TP-510-42621; NREL, Laboratory Analytical Procedure (LAP): Golden, CO, USA, 2008.
74. Sluiter, A.; Hames, B.; Ruiz, R.O.; Scarlata, C.; Sluiter, J.; Templeton, D.; Energy, D. *Determination of Structural Carbohydrates and Lignin in Biomass*; NREL/TP-510-42618; NREL, Laboratory Analytical Procedure (LAP): Golden, CO, USA, 2008.
75. Sluiter, A.; Ruiz, R.; Scarlata, C.; Sluiter, J.; Templeton, D. *Determination of Extractives in Biomass*; NREL/TP-510-42619; NREL, Laboratory Analytical Procedure (LAP): Golden, CO, USA, 2008.
76. Handy, B.E.; Sharma, S.B.; Spiewak, B.E.; Dumesic, J.A. A Tian-Calvet heat-flux microcalorimeter for measurement of differential heats of adsorption. *Meas. Sci. Technol.* **1993**, *4*, 1350–1356. [CrossRef]

Disclaimer/Publisher's Note: The statements, opinions and data contained in all publications are solely those of the individual author(s) and contributor(s) and not of MDPI and/or the editor(s). MDPI and/or the editor(s) disclaim responsibility for any injury to people or property resulting from any ideas, methods, instructions or products referred to in the content.